From particle condensation to polymer aggregation

IOP Conf. Series: Journal of Physics: Conf. Series **955** (2017) 012003 doi:10.1088/1742-6596/955/1/012003

From particle condensation to polymer aggregation

Wolfhard Janke[1] **and Johannes Zierenberg**[1,2,3]

[1] Institut für Theoretische Physik, Universität Leipzig, Postfach 100 920, 04009 Leipzig, Germany
[2] Max Planck Institute for Dynamics and Self-Organization, Am Fassberg 17, 37077 Göttingen, Germany
[3] Bernstein Center for Computational Neuroscience, Am Fassberg 17, 37077 Göttingen, Germany

E-mail: wolfhard.janke@itp.uni-leipzig.de

Abstract. We draw an analogy between droplet formation in dilute particle and polymer systems. Our arguments are based on finite-size scaling results from studies of a two-dimensional lattice gas to three-dimensional bead-spring polymers. To set the results in perspective, we compare with in part rigorous theoretical scaling laws for canonical condensation in a supersaturated gas at fixed temperature, and derive corresponding scaling predictions for an undercooled gas at fixed density. The latter allows one to efficiently employ parallel multicanonical simulations and to reach previously not accessible scaling regimes. While the asymptotic scaling can not be observed for the comparably small polymer system sizes, they demonstrate an intermediate scaling regime also observable for particle condensation. Altogether, our extensive results from computer simulations provide clear evidence for the close analogy between particle condensation and polymer aggregation in dilute systems.

1. Introduction

Condensation and nucleation processes are underlying many phenomena from galaxy evolution over cloud formation to protein aggregation. For particles or colloids much is known from experiments, theory and computation [1, 2, 3]. For polymers, the situation is less settled. At first sight, particle condensation and polymer aggregation appear to be very different processes. While condensation is a phenomenon of one's every-day-life and the stereotypic example of a first-order phase transition, aggregation is usually associated with neurodegenerative diseases such as Altzheimer's, Parkinson's, and diabetes II [4]. However, if treated outside of complex environments such as the brain, proteins in dilute solution do show cluster formation [5] with a close resemblance to classical nucleation theory [6, 7, 8]. Consequently, concepts such as nucleation rates and barriers can be qualitatively carried over to more complex macromolecular solutions [9].

There exist a lot more qualitative similarities between particle and polymer systems. For example, the phase diagrams of particle and polymer solutions appear quite similar [9, 10, 11, 12, 13, 14]. In fact, already a single polymer shows similarities to a Lennard-Jones particle cluster in its low-temperature structure [15, 16, 17]. Also, the multi-step nucleation of a few constituents to a full cluster shows a comparable hierarchy by multiple backbending in a microcanonical analysis depending on the density [18, 19, 20, 21, 22, 23]. For an abstract protein model as unit-length stick on a periodic cubic lattice the formation of fibrils shows comparable scaling

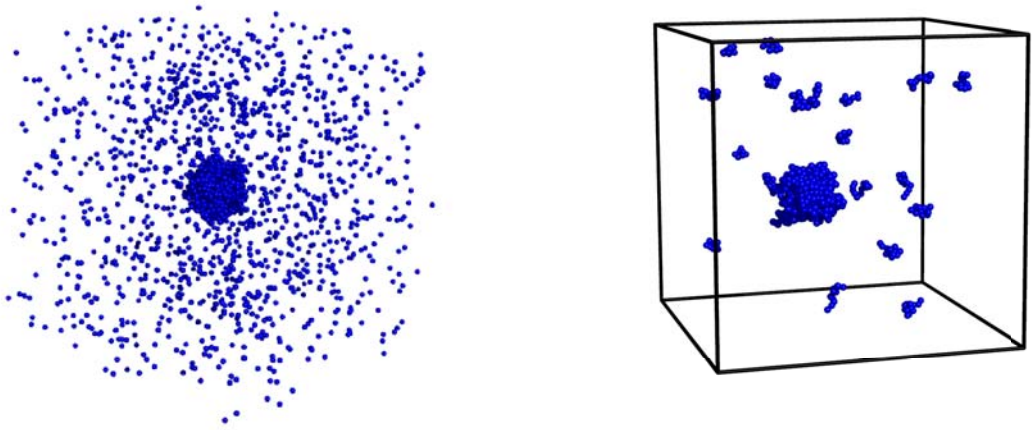

Figure 1. Illustration of droplet formation in a system of $N = 2000$ particles (left) and $N = 64$ polymers of length $P = 13$ (right).

behavior as droplet formation, which is expected since the model resembles a lattice gas with asymmetric interactions [24]. A natural question to ask is thus whether the cluster formation in polymer systems shows the same scaling behavior as in particle systems, despite their more complex structural properties [25, 26].

In this work, we want to recapitulate some evidence for an analogy between cluster formation in a particle gas and a polymer solution using a consistent model framework based on our own contributions in this field. By exploiting the similarity with particle systems, we will analyze the implications for the finite-size scaling behavior in dilute polymer systems and discuss how small system sizes may easily lead to misinterpretations.

2. Droplet formation in a particle gas

2.1. General arguments involving competition of energy and entropy at fixed temperature

Let us consider the situation of a supersaturated gas in a finite system size at fixed temperature, i.e., in the canonical (NVT) ensemble [27, 28, 29, 30, 31]. Supersaturation refers to a particle excess $\delta N = N - N_0$ compared to the temperature-specific (grand-canonical) background gas density $\rho_{\mathrm{g}}(T) = N_0(T)/V$. Besides the constant free-energy contribution from the background density, the particle excess can contribute to the system's free energy either by an entropic part from the particle fluctuations F_{fluc}, or by an energetic part F_{drop} related to the formation of a single macroscopic droplet of size V_{D}. For an illustration see Fig. 1 (left). The fluctuations can be treated in a Gaussian approximation around the equilibrium background contribution and the condensate is treated as an ideally shaped droplet [28, 29]:

$$F_{\mathrm{fluc}} = \frac{(\delta N)^2}{2\hat{\kappa}V} \qquad \text{and} \qquad F_{\mathrm{drop}} = \tau_{\mathrm{W}} V_{\mathrm{D}}^{\frac{d-1}{d}}\,, \tag{1}$$

where $\hat{\kappa} = \beta\kappa = \beta\big\langle (N - \langle N\rangle)^2\big\rangle/V$ is the isothermal compressibility and τ_{W} the surface free energy of a (Wulff shaped) droplet of unit volume.

This treatment differs from the general view on nucleation free-energy barriers, where interface free-energy loss competes with bulk free-energy gain because an infinite reservoir of attaching particles is assumed. This essentially focuses only on the droplet contribution

$\Delta F_{\rm drop} = V_{\rm D}\Delta f + \partial V_{\rm D}\sigma$, where Δf is the free-energy difference per unit volume, $\partial V_{\rm D}$ denotes the surface of $V_{\rm D}$, and σ is the surface tension. This has a clear maximum, which is obtained by solving $d\Delta F_{\rm drop}/dR = 0$ for the critical droplet radius R_c. If $R > R_c$ the droplet will grow infinitely due to the infinite reservoir of particles. In this case, R_c is not system size dependent, such that all critical droplets have the same size. We, instead, consider the equilibrium situation of a finite particle number where the gas contribution needs to be considered explicitly. For a good overview of the historical development, see, e.g., Ref. [32].

We proceed our line of arguments by linking the droplet size to the particle excess inside the droplet, $\delta N_{\rm D} = (\rho_{\rm l} - \rho_{\rm g})V_{\rm D}$, where $\rho_{\rm l}$ and $\rho_{\rm g}$ are the background liquid and gas density, respectively. General arguments show that the probability of additional intermediate-sized droplets vanishes [28, 29], so that we can distribute the particle excess in a two-phase scenario between the excess inside the droplet $\delta N_{\rm D}$ and the excess in the fluctuating phase $\delta N_{\rm F}$. In terms of the scalar fraction

$$\lambda = \delta N_{\rm D}/\delta N\,, \tag{2}$$

we obtain $\delta N_{\rm D} = \lambda\delta N$ and $\delta N_{\rm F} = (1-\lambda)\delta N$. Then, the total excess free energy $F = F_{\rm drop} + F_{\rm fluc}$ becomes

$$F = \tau_{\rm W}\left(\frac{\lambda\delta N}{\rho_{\rm l}-\rho_{\rm g}}\right)^{\frac{d-1}{d}} + \frac{(1-\lambda)^2(\delta N)^2}{2\hat{\kappa}V} = \tau_W\left(\frac{\delta N}{\rho_{\rm l}-\rho_{\rm g}}\right)^{\frac{d-1}{d}}\left(\lambda^{\frac{d-1}{d}} + \Delta(1-\lambda)^2\right), \tag{3}$$

with a dimensionless "density" parameter

$$\Delta = \frac{(\rho_{\rm l}-\rho_{\rm g})^{\frac{d-1}{d}}}{2\hat{\kappa}\tau_W}\frac{(\delta N)^{\frac{d+1}{d}}}{V} = \frac{(\rho_{\rm l}-\rho_{\rm g})^{\frac{d-1}{d}}}{2\hat{\kappa}\tau_{\rm W}}(\rho-\rho_{\rm g})^{\frac{d+1}{d}}\ V^{\frac{1}{d}}\,. \tag{4}$$

At fixed temperature, $\rho_{\rm l}, \rho_{\rm g}, \hat{\kappa}$, and τ_W are constants. By minimizing Eq. (3) with respect to λ one obtains the fraction of particles inside the largest droplet λ as a function of dimensionless density Δ, as shown for a two-dimensional lattice gas in Fig. 2 by the black "analytic" line jumping at $\Delta_{\rm c} = (1/2)(3/2)^{3/2} \approx 0.9186$ from $\lambda = 0$ to $\lambda = 2/3$. As derived in Refs. [28, 29], there exists in general a constant $\Delta_{\rm c} = \frac{1}{d}\left(\frac{d+1}{2}\right)^{\frac{d+1}{d}}$ below which no droplet forms ($\lambda = 0$) and above which a single macroscopic droplet exists with non-trivial $\lambda > \lambda_{\rm c} = \frac{2}{d+1}$. This threshold already includes the leading-order finite-size corrections, as can be seen if one rewrites Eq. (4) in terms of the density

$$\rho_{\rm c} = \rho_{\rm g} + \left(\frac{2\hat{\kappa}\tau_{\rm W}\Delta_{\rm c}}{(\rho_{\rm l}-\rho_{\rm g})^{\frac{d-1}{d}}}\right)^{\frac{d}{d+1}}\ V^{-\frac{1}{d+1}}\,. \tag{5}$$

It is less well visible that the critical droplet size $V_c = \lambda_c\delta N_c/(\rho_{\rm l}-\rho_{\rm g})$ scales non-trivially with system size, namely $V_c \propto R_c^d \propto V^{d/(d+1)}$ [27, 31, 43].

Figure 2 compares the results of simulations with the analytic prediction for a (square) lattice gas with nearest-neighbor interactions in 2D [33, 34, 35, 36]. In the lattice gas model, particles are modeled as non-empty lattice sites. This is equivalent to an Ising model, where particles correspond to either up or down spins while the vacuum corresponds to the other direction. For instance, identifying particles with up spins, the particle density ρ is related to the magnetization of the Ising model by $\rho = N/V = (1+m)/2$ and the particle gas temperature is $T = T^{\rm Ising}/4$. The data in Refs. [33, 34, 35, 36] was generated in this framework using mostly fixed-magnetization Metropolis [37] simulations (Kawasaki dynamics) at a given temperature $k_{\rm B}T = 0.375$. In two dimensions, the equivalence to the Ising model additionally provides exact results or very precise estimates for the infinite-size quantities $\rho_{\rm g}$, $\rho_{\rm l} = 1-\rho_{\rm g}$, $\hat{\kappa}$, and $\tau_{\rm W}$, necessary for the rescaling of the data according to Eq. (4) in order to compare with the theoretical (and, for the square lattice, rigorous [28, 29]) prediction [33, 34, 35, 36].

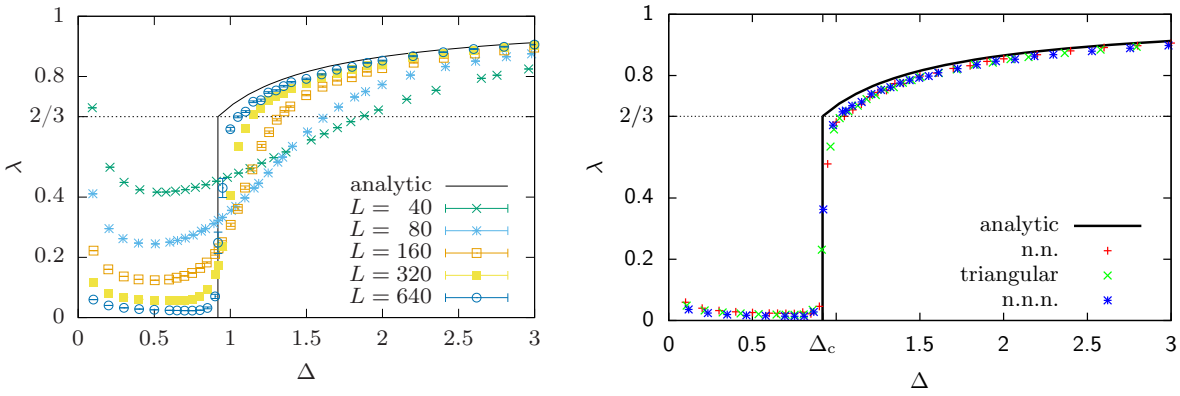

Figure 2. (left) Fraction of excess λ that goes into the droplet as a function of dimensionless rescaled density Δ for 2D droplet formation in the Ising lattice gas (square lattice with nearest-neighbor interactions) at fixed temperature $k_{\rm B}T = 0.375$ (in lattice gas normalization). Note that Δ already accounts for the leading-order finite-size scaling behavior of the density. (right) Comparison of results for three different 2D lattice gas models (nearest-neighbor (n.n.) square lattice, n.n. triangular lattice, next-nearest-neighbor (n.n.n.) square lattice) at $T \approx (2/3)T_c$ for large system size $L = 640$. Adapted from Refs. [33, 34, 35, 36].

The data in Fig. 2 (left) clearly shows that for systems of finite size the analytic solution is overestimated for low densities and (slightly) underestimated for densities above the predicted transition density Δ_c. The low-density finite-size effect is an unavoidable artefact due to the non-zero size of the largest cluster in the gas phase, which is at least $\mathcal{O}(1/N)$. The high-density deviations, on the other hand, can be attributed to physical effects such as non-ideal droplet shapes, including capillary wave distortions, and further non-trivial corrections to the theory [38]. As theoretically expected, these deviations rapidly vanish in the limit of large system size. In Refs. [34, 35] we have also checked that the analytic solution, which strictly speaking was derived for the square lattice with nearest-neighbor (n.n.) interactions in the infinite-size limit, describes other 2D lattice gases as well. This is demonstrated in Fig. 2 (right) where data for the next-neighbor triangular and next-nearest-neighbor (n.n.n.) square lattice gas are compared with the standard n.n. square lattice reference case.

Overall, Fig. 2 shows a good agreement with a surprising symmetry around Δ_c. This may be caused by a judicious choice of the fixed temperature, far enough away from the critical point to avoid strong fluctuations but high enough to avoid slow dynamics. Results for $\lambda(\Delta)$ in 3D lattice models are less symmetric, see, e.g., Ref. [39], and are currently under closer investigation. The leading-order phenomenological scaling theory of droplet formation was in general found to be consistent with numerical results for both 3D Lennard-Jones [40] and lattice [41] models.

2.2. Changing perspective to fixed density

The theory developed for fixed temperature quantitatively describes the formation and growth of a droplet with supersaturation, already including the leading-order finite-size corrections. Now, we consider instead a particle system at fixed density ρ where the temperature is lowered until a droplet forms in an *undercooled* environment, again in the canonical (NVT) ensemble as in Refs. [42, 43, 44, 45]. This can be seen as an "orthogonal" perspective in the temperature-density phase diagram of the liquid-vapor transition [43]. Considering that the "density" parameter Δ already includes the dominant or leading-order finite-size scaling behavior, we can rewrite Eq. (4) as $V^{-1/(d+1)}\Delta^{d/(d+1)} = f(\rho, \beta)$, which admits a power-series expansion in β around the infinite-size inverse temperature β_0 where $\rho_g(\beta_0) = \rho$. The

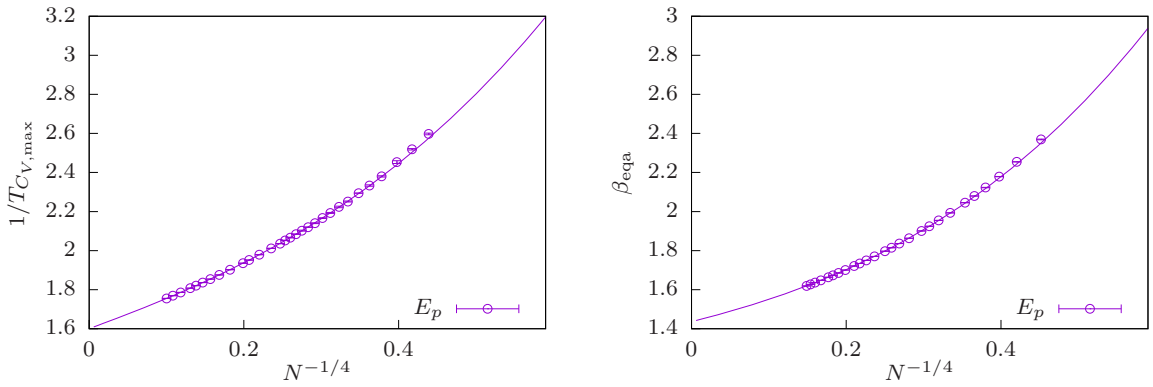

Figure 3. Finite-size scaling of the inverse transition temperature (fixed density $\rho = 10^{-2}$) for 3D droplet formation in (left) a lattice gas and (right) a Lennard-Jones gas. For the lattice gas the density is of course approximate due to discretization effects. The solid lines show fits to the ansatz (7). Adapted from Refs. [43, 45].

solution of $\Delta = \Delta_c$ then results in an asymptotic expansion in $V^{-1/(d+1)}$ for the droplet-formation point $\beta(N)$ of a finite number of particles N. Using the Taylor expansion $f(\rho,\beta) = f(\rho,\beta_0) + f'(\rho,\beta_0)(\beta-\beta_0) + \frac{1}{2}f''(\rho,\beta_0)(\beta-\beta_0)^2 + ...$, where $f(\rho,\beta_0) = 0$, one obtains

$$\beta(N) = \beta_0 + \frac{\Delta_c^{d/(d+1)}}{f'(\rho,\beta_0)} V^{-1/(d+1)} - \frac{f''(\rho,\beta_0)\Delta_c^{2d/(d+1)}}{2f'(\rho,\beta_0)^3} V^{-2/(d+1)} + \mathcal{O}\left(V^{-3/(d+1)}\right). \quad (6)$$

This of course neglects higher-order corrections to the fixed-temperature solution, especially expected non-trivial and logarithmic terms [38, 46, 47, 35, 48]. However, the scaling corrections correspond to powers of the critical droplet radius $R_c \propto V_D^{1/d} \propto V^{1/(d+1)}$ [31, 43] and we will show that fits to the higher-order terms from the Taylor expansion nicely describe the finite-size corrections in the data. Since the density is fixed, we can further replace $V \propto N$ and arrive at the ansatz for droplet formation in 3D

$$\beta(N) = \beta_0 + aN^{-1/4} + bN^{-1/2} + cN^{-3/4}. \quad (7)$$

Figure 3 shows data for droplet formation in a 3D lattice and Lennard-Jones gas based on data of Refs. [43, 45]. The lattice gas is directly treated as occupied sites on a cubic lattice with Ising-like nearest-neighbor interactions, while Lennard-Jones particles have a real-valued position in a cubic box with periodic boundary conditions interacting via the potential $V_{\rm LJ} = 4\epsilon\left[(\sigma/r)^{12} - (\sigma/r)^6\right]$ which exhibits a minimum at $r = 2^{1/6}\sigma$ of depth $-\epsilon$. Both data sets were generated using multicanonical simulations [49, 50, 51, 52] in a parallelized implementation [53, 54], which is a perfect choice for first-order-like phase transitions, especially upon variation of a continuously variable control parameter such as the temperature (for recent reviews, see Refs. [55, 56]). The parallel implementation shows linear speedup for particle condensation [39]. Canonical expectation values are obtained after a production run by standard reweighting techniques [57]. The finite-size transition temperatures $T_{C_V,\max}$ can be read off from the peak locations of the specific heat $C_V = \beta^2\left(\langle E_p^2\rangle - \langle E_p\rangle^2\right)/N$ (where E_p is the potential energy; see below) in case of the lattice gas; and from an equal-area construction in the microcanonical inverse temperature $\beta(E_p)$ [58] in case of the Lennard-Jones gas, denoted in Fig. 3 (right) by $\beta_{\rm eqa}$. Since we have no analytical solution for the infinite-size quantities $\rho(T)$, $\kappa(T)$, or $\tau_W(T)$, we merely fit the amplitudes of the correction terms in Eq. (7). In both cases, the fit qualitatively

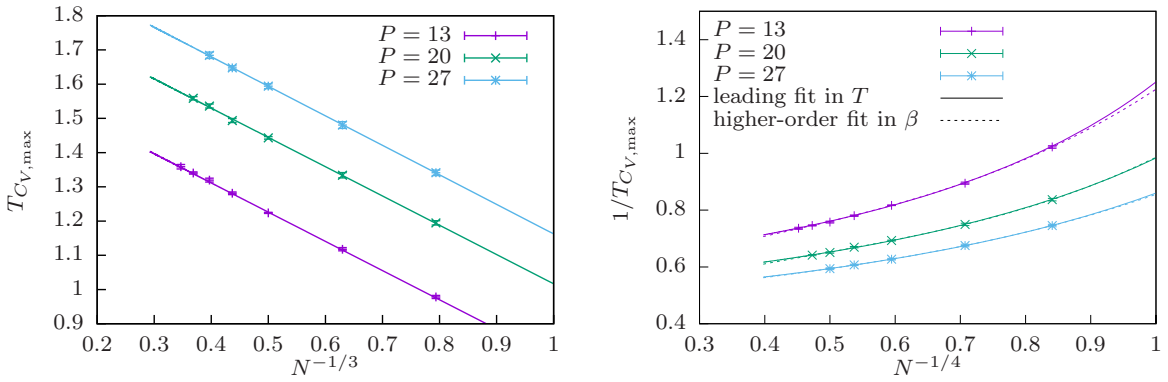

Figure 4. (left) Finite-size scaling of the transition temperature (fixed polymer density $N/V = 10^{-3}$) of cluster formation in a solution of bead-spring polymers of different length P suggests a scaling as $T - T_0 \propto N^{-1/3}$ (solid lines). (right) If the inverse temperature is instead fitted with higher-order terms the leading behavior $\propto N^{-1/4}$ is consistent with Eq. (7) (dashed lines). Adapted from Ref. [60].

describes the data very well. For the lattice gas, the fit spans $N \in [106, 10\,000]$ with a goodness-of-fit parameter $Q \approx 0.002$, attributed to the merely approximate density that one can adjust at each value of N. For the Lennard-Jones gas, the fit spans $N \in [192, 2048]$ with $Q \approx 0.5$.

Overall, the data is in good agreement with the theory on droplet formation in an undercooled gas. It is worth noting that the comparably large finite-size corrections may enable a systematic study of finite-size scaling in experimental setups on the nanoscale. If one considers argon as a model system, our largest numerical Lennard-Jones setup with 2048 particles corresponds to a box of size $L' \approx 59\ r'_{\min} = 59 \times\ 2^{1/6}\ \sigma'$ and with $\sigma' \approx 3.4\mathring{A}$ we find $L' \approx 22.5$ nm. This is a scale that both experiments and simulations may reach.

3. Droplet formation in a solution of flexible polymers

Polymers are extended objects which bring an additional conformational entropy if isolated in the high-temperature phase [59]. Lowering the temperature results in the formation of a macroscopic aggregate surrounded by a gas of isolated chains [45, 60, 61], for an illustration see Fig. 1 (right). The shape of an aggregate of flexible polymers, however, shows strong structural similarities to the droplet in a gas [16, 60], with polymers actively unfolding when incorporated into the cluster [60, 61]. If one neglects the single-polymer free-energy contributions, one may consider polymers as extended particles with a more complex, potentially temperature dependent, interaction potential. Then, it would make sense to expect the same scaling behavior for the (inverse) transition temperature as predicted for particle condensation and outlined in Sec. 2.

When treating comparably small system sizes, we noticed, however, that the scaling of the aggregation transition temperature for flexible bead-spring polymers, obtained from parallel multicanonical simulations with up to $N = 24$ polymers of length $P = 13$ ("13mers"), 20 20mers or 16 27mers, shows an apparent $T - T_0 \propto N^{-1/3}$ scaling behavior [60], see Fig. 4 (left). This appears quite puzzling in the light of our above arguments. However, inspired by the findings for polymers, a close reexamination of particle condensation revealed a prominent *intermediate scaling regime* [43], consistent with the $N^{-1/d}$ scaling behavior observed for polymers in 3D [60]. Physically this means that for a small number of constituents either none or *all* of them assemble in the droplet – the surrounding gas phase cannot really develop. The problem is, that even for particles this regime extends up to $N = 10^3 - 10^4$, also depending on the dimension [43]. This is

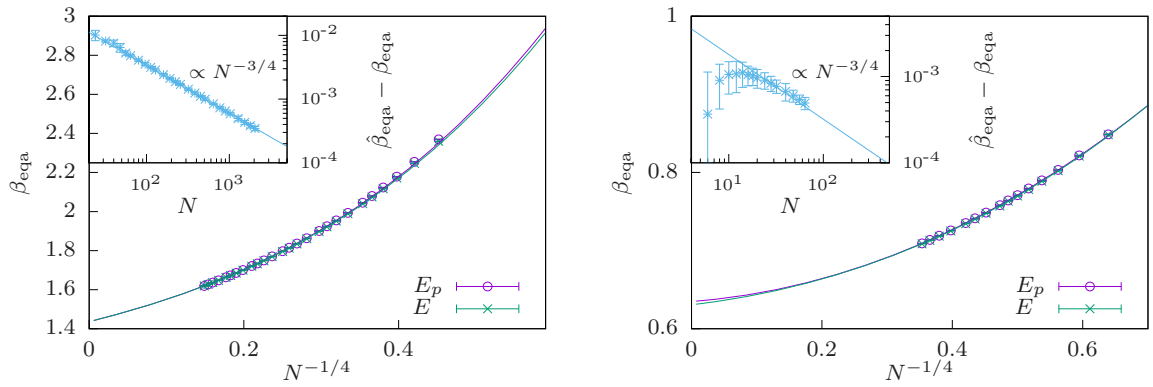

Figure 5. Finite-size scaling of the inverse transition temperatures (fixed monomer density $NP/V = 10^{-2}$) for 3D cluster formation in (left) a gas of Lennard-Jones particles and (right) a solution of flexible bead-spring polymers ($P = 13$ monomers each) reveals the same leading-order scaling as $\beta \sim N^{-1/4}$. The transition point is determined by the equal-area rule using the microcanonical inverse temperature as a function of potential energy E_p or total energy E. Adapted from Ref. [45].

out of scope even of modern simulation tools for equilibrium estimates of polymer aggregation.

One may now argue that the observation of this intermediate regime is already a first hint on an analogy between cluster formation in particle and polymer systems. In addition, we observe that the empirical corrections from Eq. (7), as powers of the critical cluster size, describe the scaling of the inverse transition temperature quite well [Fig. 4 (right), dashed lines] and is almost indistinguishable from the leading-order fit to the transition temperature [Fig. 4 (right), solid lines].

Treating larger polymer systems with up to $N = 64$ polymers of length $P = 13$ in Ref. [45] further supports the strong similarity between particles and polymers, again obtained from parallel multicanonical simulations. The inverse temperatures plotted in Fig. 5 are obtained from the equal-area construction in the microcanonical inverse temperature as a function of energy (note that a *monomer* density of 10^{-2} corresponds for 13mers to a *polymer* density of $\approx 10^{-3}$ as used in Fig. 4). Here we also emphasize a conceptual point by using both the potential energy $[\beta(E_p)]$ as used is most work using Monte Carlo simulations and the total energy $[\beta(E)]$ as considered in any textbook on statistical physics. In the latter case we analytically included the kinetic energy E_k what, technically, can be achieved by a convolution of the potential-energy probability distribution $P(E_p)$ with the Maxwell-Boltzmann distribution $P(E_k) = \frac{\beta^{3N/2}}{\Gamma(3N/2)} E_k^{(3N-2)/2} e^{-\beta E_k}$. For details see Ref. [45]. In Ref. [62] a complementary simulation method is discussed that samples directly the "real" microcanonical ensemble including the kinetic energy contribution [63, 64]. As expected both definitions show the same behavior with very small differences. It is interesting, however, that the difference between both definitions scales for large N as $\hat{\beta} - \beta \propto N^{-3/4}$, i.e., with the volume of the critical cluster [43]. This systematic behavior can be anticipated also for the case of a polymer solution. In total, this supports our hypothesis that the formation of a cluster in a dilute solution of flexible polymers can, in leading order, be described by the generic arguments derived for particle systems.

As an outlook to future work it should be stressed that biological systems usually are comprised of more complex macromolecules that cannot be assumed to be flexible. A straightforward extension of the flexible bead-spring polymer model considered above is to include worm-like chain motivated bending stiffness, leading to semiflexible homopolymers. This

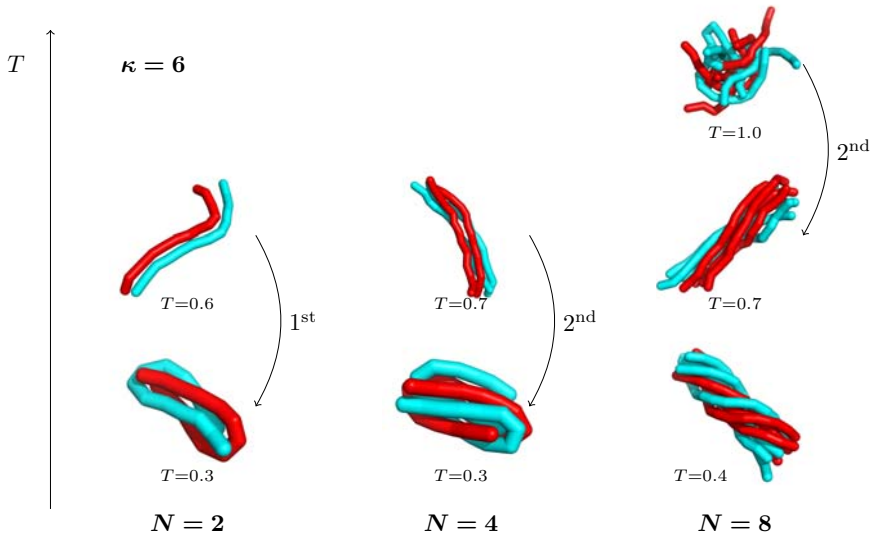

Figure 6. Typical aggregate morphologies of $N = 2, 4$, and 8 semiflexible polymers of length $P = 13$ in the intermediate-stiffness regime with bending-stiffness constant $\kappa = 6$, illustrating the size-dependence of the sub-aggregation re-ordering transitions within the aggregate: $N = 2$ polymers exhibit a first-order-like bundle-to-hairpin structural transition, whereas the finite-size transition for $N = 4$ polymers from elongated bundles to bundled hairpins is second-order-like. $N = 8$ polymers undergo a second-order-like amorphous-to-bundle transition followed by the formation of twisted bundles at even lower temperatures [65].

has an immediate impact on the structure of the low-temperature aggregate [65, 25, 26], cf. Fig. 6. While rather flexible polymers keep on forming spherical aggregates, sufficiently stiff polymers form (twisted) bundles [66, 67, 65, 25, 26] known from biopolymer systems, e.g., from amyloid protofibrils [68] or actin networks [69], or polymeric materials [70]. These bundles are not spherical but for finite diameter resemble a cylindrical structure. We do not suspect this to play an important role on the scaling of the cluster formation transition as long as the shape of the cluster does not become fractal. This is currently under active research.

4. Conclusions

In this paper we have compiled quite an extensive survey of computer simulation studies of particle condensation and polymer aggregation. By analyzing and interpreting the numerical data in a consistent theoretical framework, clear evidence for a close analogy between the cooperative behavior of particles and flexible polymers emerges.

To arrive at this main conclusion, we started with a lattice gas formulation at fixed temperature in 2D, for which we confirmed and extended in part rigorous theoretical scaling predictions in the infinite-size limit. We then proceeded to lattice and continuum Lennard-Jones particle systems in 3D, for which an "orthogonal" constant density approach was demonstrated to be more efficient. This enabled studies of large enough particle numbers to identify an intermediate scaling regime for smaller systems. Taking this crossover behavior into account we could finally show that the apparently more involved aggregation process of flexible polymers is governed by the same asymptotic scaling laws as for particles.

As an outlook we briefly mentioned on the technical side computer simulations in the "real" microcanonical ensemble that appear competitive to generalized-ensemble methods and on the

physics side the more intricate aggregation behavior of semiflexible polymers. In general, our approach can be extended to elucidate nucleation mechanisms including nucleation barriers and rates in greater detail. These topics appear to be promising avenues for future work.

Acknowledgments
This work has been partially supported by the Deutsche Forschungsgemeinschaft (DFG) under Grant No. JA 483/31-1 and SFB/TRR 102 (project B04), the Leipzig Graduate School of Natural Sciences "BuildMoNa", the Deutsch-Französische Hochschule DFH-UFA through the Doctoral College "$\mathbb{L}^4$" under Grant No. CDFA-02-07, and the EU Marie Curie IRSES network DIONICOS under Contract No. PIRSES-GA-2013-612707. JZ received financial support from the German Ministry of Education and Research (BMBF) via the Bernstein Center for Computational Neuroscience (BCCN) Göttingen under Grant No. 01GQ1005B.

References
[1] Kelton K F and Frenkel D 2016 *J. Chem. Phys.* **145** 211501
[2] Binder K and Virnau P 2016 *J. Chem. Phys.* **145** 211701
[3] Herlach D M, Palberg T, Klassen I, Klein S and Kobold R 2016 *J. Chem. Phys.* **145** 211703
[4] Chiti F and Dobson C M 2006 *Annu. Rev. Biochem.* **75** 333
[5] Stradner A, Sedgwick H, Cardinaux F, Poon W C K, Egelhaaf S U and Schurtenberger P 2004 *Nature (London)* **432** 492
[6] Feder J, Russell K C, Lothe J and Pound G M 1966 *Adv. Phys.* **15** 111
[7] Oxtoby D W 1992 *J. Phys: Condens. Matter* **4** 7627
[8] Kashchiev D 2000 *Nucleation: Basic Theory with Applications* (Oxford: Butterworth-Heinemann)
[9] Sear R P 2007 *J. Phys.: Condens. Matter* **19** 033101
[10] Wilding N B 1995 *Phys. Rev.* E **52** 602
[11] Wilding N B 1997 *J. Phys.: Condens. Matter* **9** 585
[12] MacDowell L G, Virnau P, Müller M and Binder K 2002 *J. Chem. Phys.* **117** 6360
[13] Virnau P, Müller M, MacDowell L G and Binder K 2004 *New J. Phys.* **6** 7
[14] Virnau P, Müller M, MacDowell L G and Binder K 2004 *J. Chem. Phys.* **121** 2169
[15] Schnabel S, Vogel T, Bachmann M and Janke W 2009 *Chem. Phys. Lett.* **476** 201
[16] Schnabel S, Bachmann M and Janke W 2009 *J. Chem. Phys.* **131** 124904
[17] Schnabel S, Janke W and Bachmann M 2011 *J. Comp. Phys.* **230** 4454
[18] Junghans C, Bachmann M and Janke W 2006 *Phys. Rev. Lett.* **97** 218103
[19] Junghans C, Bachmann M and Janke W 2008 *J. Chem. Phys.* **128** 085103
[20] Junghans C, Bachmann M and Janke W 2009 *Europhys. Lett.* **87** 40002
[21] Junghans C, Bachmann M and Janke W 2011 *Comput. Phys. Commun.* **9** 1937
[22] Schierz P, Zierenberg J and Janke W 2015 *J. Chem. Phys.* **143** 134114
[23] Koci T and Bachmann M 2017 *Phys. Rev.* E **95** 032502
[24] Irbäck A and Wessén J 2015 *J. Chem. Phys.* **143** 105104
[25] Zierenberg J, Marenz M and Janke W 2016 *Polymers* **8** 33
[26] Janke W, Marenz M and Zierenberg J 2017 *Lobachevskii J. Math.* **38** 978
[27] Binder K and Kalos M H 1980 *J. Stat. Phys.* **22** 363
[28] Biskup M, Chayes L and Kotecký R 2002 *Europhys. Lett.* **60** 21
[29] Biskup M, Chayes L and Kotecký R 2003 *Commun. Math. Phys.* **242** 137
[30] Neuhaus T and Hager J S 2003 *J. Stat. Phys.* **113** 47
[31] Binder K 2003 *Physica* A **319** 99
[32] Schrader M, Virnau P and Binder K 2009 *Phys. Rev.* E **79** 061104
[33] Nußbaumer A, Bittner E, Neuhaus T and Janke W 2006 *Europhys. Lett.* **75** 716
[34] Nußbaumer A, Bittner E and Janke W 2008 *Phys. Rev.* E **77** 041109
[35] Nußbaumer A, Bittner E and Janke W 2010 *Prog. Theor. Phys. Suppl.* **184** 400
[36] Nußbaumer A, Zierenberg J, Bittner E and Janke W 2016 *J. Phys.: Conf. Series* **759** 012009
[37] Metropolis N, Rosenbluth A W, Rosenbluth M N, Teller A H and Teller E 1953 *J. Chem. Phys.* **21** 1087
[38] Kotecký R *Private communication*
[39] Zierenberg J, Wiedenmann M and Janke W 2014 *J. Phys.: Conf. Series* **510** 012017
[40] MacDowell L G, Virnau P, Müller M and Binder K 2004 *J. Chem. Phys.* **120** 5293
[41] Schmitz F, Virnau P and Binder K 2013 *Phys. Rev.* E **87** 053302

[42] Martinos S, Malakis A and Hadjiagapiou I 2007 *Physica* A **384** 368
[43] Zierenberg J and Janke W 2015 *Phys. Rev.* E **92** 012134
[44] Zierenberg J and Janke W 2016 *J. Phys.: Conf. Series* **750** 012017
[45] Zierenberg J, Schierz P and Janke W 2017 *Nat. Commun.* **8** 14546
[46] Langer J S 1967 *Ann. Phys. N.Y.* **41** 108
[47] Ryu S and Cai W 2010 *Phys. Rev.* E **81** 030601(R)
[48] Prestipino S, Laio A and Tosatti E 2012 *Phys. Rev. Lett.* **108** 225701
[49] Berg B A and Neuhaus T 1991 *Phys. Lett.* B **267** 249
[50] Berg B A and Neuhaus T 1992 *Phys. Rev. Lett.* **68** 9
[51] Janke W 1992 *Int. J. Mod. Phys.* C **3** 1137
[52] Janke W 1998 *Physica* A **254** 164
[53] Zierenberg J, Marenz M and Janke W 2013 *Comput. Phys. Commun.* **184** 1155
[54] Zierenberg J, Marenz M and Janke W 2014 *Physics Procedia* **53** 55
[55] Janke W and Paul W 2016 *Soft Matter* **12** 642
[56] Berg B A 2017 *Eur. Phys. J. Special Topics* **226** 551
[57] Janke W 2003 *Histograms and all that* in *Computer Simulations of Surfaces and Interfaces* NATO Science Series II. Mathematics, Physics and Chemistry – Vol. 114 ed by B Dünweg, D P Landau and A I Milchev (Dordrecht: Kluwer) pp 137–157
[58] Janke W 1998 *Nucl. Phys.* B (Proc. Suppl.) **63A-C** 631
[59] de Gennes P-G 1979 *Scaling Concepts in Polymer Physics* (Ithaca: Cornell University Press)
[60] Zierenberg J, Mueller M, Schierz P, Marenz M and Janke W 2014 *J. Chem. Phys.* **141** 114908
[61] Mueller M, Zierenberg J, Marenz M, Schierz P and Janke W 2015 *Physics Procedia* **68** 95
[62] Schierz P, Zierenberg J and Janke W 2016 *Phys. Rev.* E **94** 021301(R)
[63] Calvo F, Neirotti J P, Freeman D L and Doll J D 2000 *J. Chem. Phys.* **112** 10350
[64] Martín-Mayor V 2007 *Phys. Rev. Lett.* **98** 137207
[65] Zierenberg J and Janke W 2015 *Europhys. Lett.* **109** 28002
[66] Kierfeld J, Kühne T and Lipowsky R 2005 *Phys. Rev. Lett.* **95** 038102
[67] Heussinger C, Schüller F and Frey E 2010 *Phys. Rev.* E **81** 021904
[68] Giurleo J T, He X and Talaga D S 2008 *J. Mol. Biol.* **381** 1332
[69] Pandolfi R J, Edwards L, Johnston D, Becich P and Hirst L S 2014 *Phys. Rev.* E **89** 062602
[70] Kouwer P H, Koepf M, Le Sage V A, Jaspers M, van Buul A M, Eksteen-Akeroyd Z H, Woltinge T, Schwartz E, Kitto H J, Hoogenboom R, Picken S J, Nolte R J, Mendes E and Rowan A E 2013 *Nature (London)* **493** 651